ACS APPLIED MATERIALS & INTERFACES

Research Article

www.acsami.org

Stable Conjugates of Peptides with Gold Nanorods for Biomedical Applications with Reduced Effects on Cell Viability

Carolina Adura,[†,‡] Simon Guerrero,[‡] Edison Salas,[†] Luis Medel,[‡] Ana Riveros,[‡] Juan Mena,[‡] Jordi Arbiol,[§,∥] Fernando Albericio,[⊥,⊗,○,#] Ernest Giralt,[⊥,⊗] and Marcelo J. Kogan*[,‡]

[†]Facultad de Química y Biología, Universidad de Santiago de Chile, Santiago, Chile

[‡]Facultad de Ciencias Químicas y Farmacéuticas, Universidad de Chile, Santiago, Chile

[§]Institut de Ciència de Materials de Barcelona, ICMAB-CSIC, Bellaterra, 08193, CAT, Spain

[∥]Institució Catalana de Recerca i Estudis Avançats (ICREA), 08010 Barcelona, CAT, Spain

[⊥]Institute for Research in Biomedicine, IRB Barcelona, 08028-Barcelona, Spain

[⊗]Department of Organic Chemistry, University of Barcelona, 08028-Barcelona, Spain

[○]CIBER-BBN Networking Centre on Bioengineering, Biomaterials, and Nanomedicine, Barcelona Science Park, 08028-Barcelona, Spain

[#]School of Chemistry and Physics, University of KwaZulu-Natal, 4001-Durban, South Africa

Supporting Information

ABSTRACT: Gold nanorods used in therapy and diagnosis must be nontoxic and stable in biological media and should be specific for the target. The complete combination of these three factors has hindered the use of gold nanorods as carriers in biological and biomedical applications. In this study, we produced a conjugate of gold nanorods with the peptide CLPFFD that recognizes toxic β-amyloid aggregates present in Alzheimer's disease, demonstrates colloidal stability, maintains plasmonic properties, and shows no effects on cell viability in the SH-SY5Y cell line. Furthermore, the irradiation of β-amyloid in the presence of the conjugate with near-infrared region irradiation energy reduces the amyloidogenic process reducing also its cytotoxicity. The nanorods were synthesized following the seed-mediated method in cetyltrimethylammonium bromide (CTAB) and were conjugated with the N-terminal cysteine peptide, CLPFFD. The conjugate was exhaustively characterized using different techniques (Absorption spectroscopy, X-ray photoelectron spectroscopy, electron energy loss spectroscopy, and zeta potential). The effects on cell viability and cell penetration by transmission electron microscopy of the conjugate were evaluated. The chemisorption of the peptide on the surface of gold nanorods increases their stability and reduces their effects on cell viability.

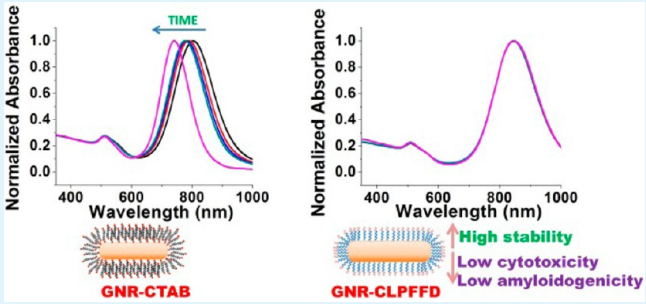

KEYWORDS: *gold nanorods, peptide, stability, cell viability, Alzheimer's disease, amyloidogenesis, NIR irradiation*

INTRODUCTION

Nanotechnology offers enormous potential for diagnostics and therapy. Because of their optical and electric properties,[1] different types of gold nanoparticles (GNPs) have been studied for biomedical applications,[2−6] including imaging,[7,8] biosensing,[9,10] and the delivery of either genes[11,12] or antitumor drugs for cancer diagnosis and therapy.[13]

In previous work on Alzheimer's disease, we found that is it possible to locally and remotely destroy toxic aggregates of β-amyloid (Aβ) after microwave irradiation in the presence of gold nanospheres.[6,14] We conjugated spherical GNPs to the amphipathic peptide CLPFFD that recognizes Aβ. The conjugation increased the stability of the nanoparticles through a steric effect and favored the crossing of the blood-brain barrier. On the other hand, Huo et al demonstrated that it is possible to destroy toxic aggregates of Aβ by photothermal ablation in the presence of GNPs.[15] Alzheimer's disease (AD) is the most common cause of dementia, affecting 33.9 million people worldwide.[16] AD is characterized by the presence of dense extraneuronal protein deposits (amyloid plaques) and intraneuronal fibrous features (neurofibrillary tangles).[17] The aggregation of Aβ is closely related to the neurodegeneration and development of AD and is central to the neurodegeneration that produces amyloid plaques.[18] Recently, several authors hypothesized that the key to an early pathogenic event in the onset of AD is conversion of the monomeric form of Aβ into prefibrillar intermediate amyloidogenic aggregates (PIAA) as oligomers,amylospheroids (AS), protofibrils (PF), pores, and

Received: November 27, 2012
Accepted: April 18, 2013
Published: April 18, 2013

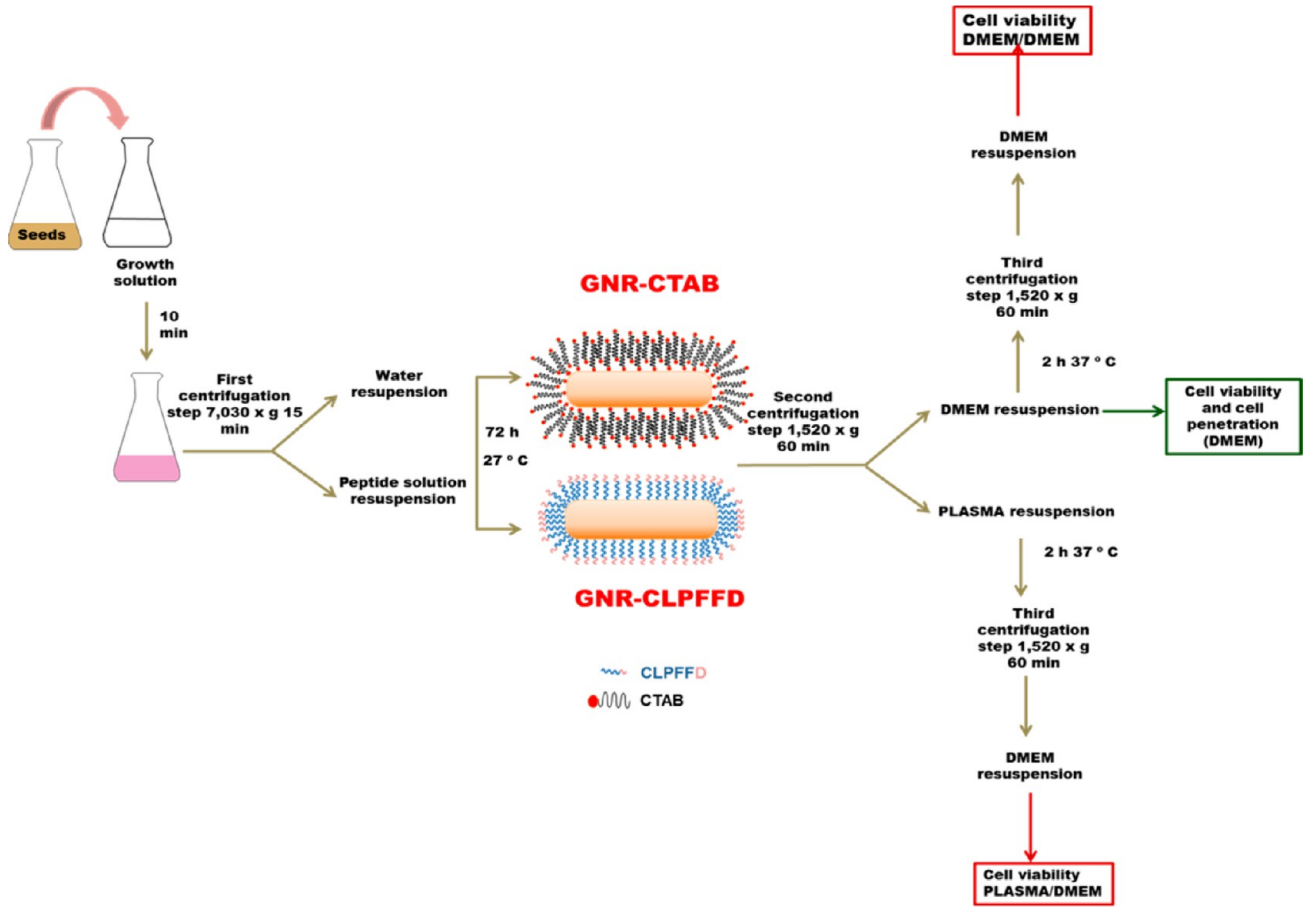

Figure 1. Schematic representation of the synthesis and preparation of GNRs samples for biological experiments.

short fibrils (SF). A strategy for treating the disease could be reducing the amyloidogenicity of PIAA.[19] For early stages of AD, this inhibition is of major importance in developing a potential treatment strategy.

Nanoparticles formed by noble metals can absorb photons, dissipating the absorbed energy and producing local heating because of the surface plasmon resonant effect (SPR).[20] The SPR effect occurs in gold nanorods (GNRs) with appropriate aspect ratios (length/width) at wavelengths in the NIR region (700−1300 nm), which is especially appropriate for biomedical applications because tissues and cells have lower absorption coefficients (680−900 nm) in this region.[21] With GNRs, it is possible to efficiently convert NIR radiation to local (few nanometers) heating with minimal adverse effect on cells.

GNRs that are used in therapy and diagnosis must be nontoxic, stable in biological media, and specific to the target. These three requirements have limited the use of GNRs as carriers in biological and biomedical applications. The synthesis of GNRs requires the presence of a high concentration (approximately 0.1 M) of cetyltrimethylammonium bromide (CTAB) that favors the asymmetric geometry.[22] However, CTAB is known to degrade biomembranes, raising a significant concern about the cytotoxicity of GNR-CTAB in vitro and in vivo.[23−28] The cytotoxic effects of GNR-CTAB can be minimized by reducing the CTAB concentration below the critical micellar concentration,[29] but this reduction occurs at the expense of the stability of the nanorod suspension, consequently compromising their unique optical properties in biological environments.[30]

GNRs have been capped with different molecules to increase their stability.[27,28,31] However, biocompatibility has not been addressed. Polyelectrolyte-coating schemes have been used to coat GNRs.[27,32] Recently, biologically functional cationic GNR-phospholipids with carrier capabilities also exhibited improved colloidal stability, maintained plasmonic properties, and showed no cytotoxicity under physiological conditions.[30]

For this study, we obtained a conjugate of GNRs with the CLPFFD peptide that simultaneously had the following attributes: selective binding to β-amyloid aggregates, colloidal stability, plasmonic properties, and no effects on cell viability in neuroblastoma cells. Furthermore, NIR irradiation of amyloidogenic species of β-amyloid in the presence of GNRs capped with CLPFFD (GNR-CLPFFD) reduced the amyloidogenic capacity of PIAA and their citotoxicity after incubation. First, we exhaustively characterized the GNR-CLPFFD and demonstrated that GNR-CLPFFD is stable in physiological media and thus retains its unique plasmonic properties. On the basis of studies of viability, cytotoxicity, and cell proliferation, we demonstrated that the GNR-CLPFFD conjugate did not affect cell viability, in contrast to GNR-CTAB.

EXPERIMENTAL PROCEDURES

Synthesis of the Peptide CLPFFD. CLPFFD was synthesized following protocols described previously in references 6 and 14.

Preparation of GNR-CTAB. GNR-CTABs were synthesized using the seed-mediated approach.[33] In the first step, a seed solution was prepared to reduce 250 μL of $HAuCl_4$ in a solution of 9.75 mL of 0.1 M CTAB and cold-prepared sodium borohydrate (600 μL, 0.01 M). Seeds were kept at 27 °C for 2 h before use. Next, 55 μL of 0.1 M

dx.doi.org/10.1021/am3028537 | ACS Appl. Mater. Interfaces 2013, 5, 4076−4085

ascorbic acid was added to a growth solution containing 75 μL of 0.01 M $AgNO_3$, 9.5 mL of 0.1 M CTAB, and 500 μL of $HAuCl_4$ 0.01 M. Then, 250 μL of HCl 0.1 M and 12 μL of the previously prepared seed solution were added. The solution was allowed to react for 10 min at 27 °C before centrifugation at 7,030*g* for 15 min (first centrifugation step, Figure 1). After centrifugation, the supernatant was removed, and the pellet was resuspended in milli-Q water. Vis-NIR absorption spectra were recorded at room temperature with a 2501PC UV−vis recording spectrophotometer (Shimadzu Corporation, Kyoto, Japan). GNRs were observed using transmission electron microscopy (TEM) with a JEOL JEM-1010 microscope. The specimen was prepared by dropping GNRs on Formvar carbon-coated copper microgrids and letting them dry.

Conjugation of GNRs with CLPFFD. For conjugation of CLPFFD to GNRs, GNRs were prepared as described above and after the first centrifugation step (see Figure 1), the pellets to prepare GNR-CLPFFD (pellets that come from 4 mL of original GNR-CTAB solution) were resuspended in 4 mL of an aqueous peptide solution in a concentration of 0.25 mg/mL, and the final mixture was allowed to react for 72 h at 27 °C.

Calculation of GNR Concentration. An aliquot of a known volume of GNRs solution was lyophilized, and the gold content was determined by neutron activation analysis (NAA) determining the gold concentration C_{Au} (Chilean Nuclear Energy Commission, CCHEN). The samples were sealed by friction welding and exposed for 17 h to a neutron flux of 0.25−1.3 n/cm^2 s with a power of 5 mW using a RECH-1 reactor at the Chilean Nuclear Energy Commission, CCHEN, thereby triggering the conversion of ^{197}Au to ^{198}Au. After 7−12 days of neutron bombardment, the γ-rays emitted by the samples were counted and sorted by energies using a germanium detector coupled to a PC-based multichannel γ-ray spectrometer. The γ-spectra were analyzed using the software SAMPO90 Canberra. Gold standards were run with the experimental samples to standardize a library of gold element data from which the amount of gold present in the unknowns was calculated.

The final uncertainty is evaluated by combining the individual components with that contributed by neutron activation: μ-weight of the sample, μ-weight of the standard reference material, μ-measure of the analyte in the sample, μ-measure of the analyte in the standard, μ-neutron flux of the standard reference material, μ-neutron flux of the sample, and μ correction of the dead time in the sample and in the standard reference material. The uncertainty informed corresponds to the uncertainty expanded (U), which was calculated with a cover factor equal to 2. This factor is equivalent to a level of confidence of 95%.

With the C_{Au} data and knowing the length and width averages of the GNR (both determined by TEM), the concentration (nanomolar) of GNR was determined as follows:[34]

$$\mathrm{CGNR} = 4 \times C_{Au}/\rho_{Au} \times \pi \times W \times 2L$$

where CGNR is the GNR concentration, ρ_{Au} is the density of gold atoms in the bulk (59 atoms/nm^3), C_{Au} is the gold concentration determined by gold neutron activation, L is the length of GNR determined by TEM, and W is the width of GNR determined by TEM.

Estimation of the Number of Peptide Molecules per GNR. The number of peptide molecules per GNR was estimated by amino acids analysis and NAA. The concentration of GNR in solution was determined by NAA and TEM while the peptide concentrations were obtained by amino acid analysis after centrifugation at 16,560*g* for 30 min of the GNR. In such conditions the GNRs sediment out, and the number of peptide molecules per GNR was calculated by dividing the number of peptide molecules per mL of solution by the number of particles per mL of solution (obtained as was explained in the previous section). This ratio was obtained in triplicate in three independent analyses.

To determine the quantity of peptide molecules that are bound to GNR, a GNR-CLPFFD solution was lyophilized and hydrolyzed for 72 h in 6 N HCl with a known quantity of amino butyric acid as internal standard. Afterwards, the solution was evaporated under reducing pressure and derivatized for the amino acid analysis by HPLC.

Preparation of GNR Samples for Biological Studies. For the biological studies, excess of the free peptide was eliminated, and the level of CTAB was reduced by centrifugation of 1 mL of the solution at 1,520*g* for 60 min (second centrifugation step, Figure 1). Finally, the pellets were resuspended as follows:

(a) In 4 mL of DMEM low-glucose medium (Biological Industries) containing 10% inactivated fetal calf serum (FCS), (this sample is called DMEM in Figure 7).

(b) In 1 mL of human plasma, followed by incubation for 2 h at 37 °C and then centrifugation at 1,520*g* for 60 min (third centrifugation step, Figure 1). The pellet was reconstituted in 1 mL of DMEM low-glucose medium (Biological Industries) containing 10% inactivated fetal calf serum (FCS), (this sample is called PLASMA/DMEM in Figure 7).

(c) In 1 mL of DMEM, followed by incubation and then centrifugation at 1,520*g* for 60 min (third centrifugation step, Figure 1). The pellet was reconstituted in 1 mL of DMEM supplemented with 10% inactivated fetal bovine serum (this sample is called DMEM/DMEM in Figure 7 and the same sample was called DMEM/DMEM nonirradiated [DMEM/DMEM (NI), Supporting Information, Figure S13].

(d) The sample DMEM/DMEM was irradiated and incubated with the cells. The sample was called DMEM/DMEM (I) (Supporting Information, Figure S13).

(e) The sample DMEM/DMEM was centrifuged, and the supernatant was incubated with the cells. The sample was called DMEM/DMEM (SNI) (Supporting Information, Figure S13).

(f) The sample DMEM/DMEM was irradiated, centrifuged, and the supernatant was incubated with the cells. The sample was called DMEM/DMEM (Supporting Information, Figure S13).

Stability of the GNR-CTAB, GNR-CLPFFD, and GNR-CLPFFD in Biological Media. The stability of GNR-CTAB and GNR-CLPFFD was evaluated following Vis-NIR spectra at room temperature until 72 h after synthesis. Otherwise, for the samples DMEM, DMEM/DMEM, and PLASMA/DMEM the cell medium without pH indicator was used, and samples were incubated for 24 h at 37 °C. In all the cases DMEM without pH indicator was used as a blank for spectrophotometric measurements.

Electron Energy Loss Spectroscopy (EELS) of STEM Images. For obtaining the sulfur EELS profile of GNR-CLPFFD samples (S L2,3-edge placed at 165 eV), a drop of GNR-peptide was deposited on a Holey carbon-coated 400 mesh Cu grid. Then, we used a Gatan Image Filter (GIF 2001) coupled to a JEOL 2010F microscope with an energy resolution of approximately 1.2 eV. The microscope was operated in the scanning TEM mode using a high-angle annular dark field (HAADF) detector.

X-ray Photoelectron Spectroscopy (XPS). XPS experiments were performed using a PHI 5500 Multitechnique System (from Physical Electronics) with a monochromatic X-ray source (Al KR line of 1486.6 eV energy and 350 W) that was placed perpendicular to the analyzer axis and calibrated using the $3d_{5/2}$ line of Ag with a full width at half-maximum (fwhm) of 0.8 eV. The analyzed area was a circle of 0.8 mm in diameter, and the selected resolution for the general spectra was 187.5 eV of pass energy and 0.8 eV/step; the resolution for the spectra of the different elements was 23.5 eV of pass energy and 0.1 eV/step. Some measurements were conducted after cleaning the surface by sputtering with an Ar^+ ion source (4 keV energy). All measurements were performed in an ultrahigh-vacuum chamber with a pressure between 5×10^{-9} and 2×10^{-8} Torr.

Zeta Potential. The zeta potential (Zeta sizer 3000, Malvern Instruments, U.K.) measurements of nanoparticles consisted of five repeats of each GNR solution. Since the zeta potential measurements were performed in an aqueous solution, the Smolochowski approximation was used to calculate the zeta potential from the electrophoretic mobility measured. The electrophoretic determinations of zeta potential are most commonly made in aqueous media and a moderate electrolyte concentration.

Interaction of GNR-CLPFFD with Amyloid Fibrils. $A\beta_{1-42}$ was purchased from r-Peptide. Aβ was dissolved in water, aliquoted, lyophilized and stored in glass vials at −20 °C until used. To obtain

mature Aβ fibrils, the aliquots were treated with 1,1,1,3,3,3-hexafluoro-2-propanol (HFIP) for 30 min to give the monomeric Aβ form. Aliquots were then lyophilized and resuspended in GNR-CLPFFD solution (0.2 nM approx.). The final Aβ concentration was 26 μM. The samples were incubated for 5 days at 37 °C with mechanical shaking. For TEM observations the samples were adsorbed for 1 min onto glow discharged carbon-coated colloidal films on 200 mesh copper grids. The TEM grids were then blotted and washed in Milli-Q water before negative staining with 2% uranyl acetate for visualization by TEM (JEOL JEM-1010).

Quantification of Gold in Fibrils and Supernatants. To separate the free and bound GNR-CLPFFD a centrifugation at 380*g* for 20 min was carried out. The pellet was washed with water, and the first and the second supernatant were mixed. The content of gold in both pellet and supernatant after liophilization was analyzed by NAA. The determinations were carried out in triplicate.

Preparation of Aβ PIAA Solutions. $A\beta_{1-42}$ was purchased from r-Peptide (U.S.A.). About 1 mg peptide was suspended in water (1 mL), and this suspension was divided in 10 aliquots. Peptide aliquots were lyophilized in glass vials and stored at −20 °C. To obtain an homogeneous Aβ solution free from aggregates, the peptide was treated with 200 μL of 1,1,1,3,3,3-hexafluoro-2-propanol for 30 min at room temperature. The HFIP was then lyophilized, and the peptide was dissolved in water to obtain a 400 μM solution of Aβ PIAA.[35]

Evaluating the Amyloidogenic Process. Irradiation and Incubation of PIAA in the Presence of GNR-CLPFFD. First, for the sample preparation 20 μL of a solution of PIAA was mixed with 380 μL of a GNR-CLPFFD solution (0.1 nM final concentration of GNR-CLPFFD) and for the control 20 μL of a solution of PIAA was mixed with 380 μL of a supernatant of a centrifuged solution of GNR-CLPFFD (1,520*g* for 60 min). Next, the samples and controls were incubated for 25 min at room temperature. The sample and control were divided into two aliquots. One aliquot was irradiated with an 808 nm, 450 mW continuous laser (Power Technology Inc.). Afterward, 200 μL of each sample was placed in a plastic cuvette and irradiated continuously for 5, 20, or 120 min. Immediately after the irradiation, the samples were placed in a thermomixer for 24 h at 37 °C and 300 rpm. After that, to detect amyloid fibrils the thioflavin-T assay was performed, and the samples were placed in a black 96-well plate with 0.5 M glycine buffer with a pH of 8.4 and 0.1 M thioflavin-T. The samples were measured with excitation at 450 nm and emission at 480 nm.

Interaction of GNR-CLPFFD with Albumin Fibrils. Bovine serum albumin (BSA) was dissolved in 10 mM phosphate buffer at pH 7.4 with 10 mM NaCl. The BSA solution was mixed with a solution of GNR-CLPFFD (0.4 nM) (the concentration was set to 30 μM for the protein and 0.2 nM for the GNR-CLPFFD). The samples were incubated for 48 h and for 5 d at 65 °C with mechanical shaking at 300 rpm.[36] The extent of BSA fibrillation was monitored using the thioflavin-T fluorescence. For TEM images, the samples were adsorbed for 1 min onto glow-discharged carbon-coated colloidal films on 200-mesh copper grids.

Cell Viability Assay. SH-SY5Y cell line was maintained in DMEM low-glucose medium (Biological Industries) containing 10% inactivated fetal calf serum (FCS), 2 mM glutamine, 50 U/mL penicillin, and 0.05 g/mL streptomycin.

To determine the effect of the GNRs on cell viability, a 3-(4,5-dimethylthiazol-2-yl)-5-(3-carboxymethoxyphenyl)-2-(4-sulfophenyl)-2*H*-tetrazolium (MTS) assay was performed which permitted the establishment of a linear relationship between the viable cell number and absorbance. For the MTS assay, the SH-SY5Y cells were seeded on 96-well plates at 2500 cells per well in Dulbecco's modified Eagle's medium, with phenol red. The cells were then treated with increasing concentrations of GNRs. After 48 h of incubation, cell viability was measured (in triplicate) in three independent experiments using the MTS assay according to manufacturer's protocol. Briefly, MTS tetrazolium salt needs an electron coupling reagent (phenazine methosulfate; PMS), MTS and PMS are dissolved in Dulbecco's phosphate buffered saline (DPBS) with an optimal pH in 6−6.5 range, the MTS and PMS are mixed to obtain in the assay 333 μg/mL MTS and 25 μM PMS and added to the cells before the end of the experiment for a range of 1 to 3 h at 37 °C. The absorbance at 490 nm was read on a Multiscan reader with reference wavelength of 655 nm.

GNR-CLPFFD Cell Penetration. Neuroblastoma cells SH-SY5Y were incubated with GNR-CLPFFD for 24 h. Cells were fixed with 2.5% glutaraldehyde in phosphate buffer and then kept in the fixative at 4 °C for 24 h. The cells were then washed with the phosphate buffer and postfixed with 1% osmium tetraoxide using the same buffer that contained 0.8% potassium ferricyanide at 4 °C. The samples were then dehydrated in acetone, infiltrated with Epon resin for 2 days, embedded in the resin, and polymerized at 60 °C for 48 h. Ultrathin sections were obtained using a Leica Ultracut UCT ultramicrotome and mounted on Formvar-coated copper grids. The sections were stained with 2% uranyl acetate in water and lead citrate and then observed under a JEM-1010 electron microscope (JEOL, Japan).

Effects of Irradiated PIAA with NIR in the Presence of the GNR-CLPFFD on Neurons Viability. *Hippocampal Neuron Culture.* Primary rat hippocampal cells from Sprague−Dawley rats at embryonic day 18 were prepared as described.[37] Briefly, hippocampus was dissected in Hank's balanced salt solution with 10 mM Hepes, pH 7.4, and 0.5% glucose (HBSS). After, the tissue was resuspended in HBSS containing 0.25% trypsin and incubated for 20 min at 37 °C. After, the tissue was mechanically dissociated in DMEM low-glucose medium (Biological Industries) containing 10% inactivated fetal bovine serum (FBS), 50 U/mL penicillin, and 0.05 g/mL streptomycin. Hippocampal cells were seeded on 96-well plates at 60,000 cells per well in polylysine coated plates and maintained Neurobasal medium, supplemented with B27, for 6 days before the cell treatments.

Irradiation of Aβ PIAA/GNR-CLPFFD. Immediately before use, the HFIP-treated Aβ was dissolved in dimethylsulfoxide (DMSO) and diluted in phosphate-buffered saline (PBS, pH 7.4) to obtain a 400 μM solution of Aβ PIAA. The solution of PIAA was mixed with the GNR-CLPFFD solution (0.4 nM) to obtain a 100 μM solution of Aβ PIAA. The samples were then divided into two aliquots. One aliquot was irradiated with an 808 nm, 450 mW continuous laser (Power Technology Inc.). Each sample was then placed in a plastic cuvette and irradiated continuously for 2 h. Immediately after the irradiation, the hippocampal cells were treated with Aβ PIAA/GNR-CLPFFD (irradiated and nonirradiated) samples. The final concentration of Aβ in the cells was 10 μM. The same volume of medium with GNR-CLPFFD was added to the control. The hippocampus cells were then incubated for 24 h at 37 °C. Cell viability was measured (in triplicate) using the modified MTS assay.

RESULTS AND DISCUSSION

Design of the Conjugate GNR-CLPFFD. We conjugated GNRs with the amphipathic peptide CLPFFD (Supporting Information, Figure S1) that is derived from the Aβ peptide sequence and recognizes it. At the C-terminal extreme, the peptide CLPFFD contains an Asp residue (D) that increases peptide solubility and confers primary amphipathicity to the molecule. Amphipathicity refers to a polar charge at the C-terminal end of the sequence and predominately hydrophobic residues at the end of the sequence. The presence of the residues Leu (L) and Phe (F), also found in the native sequence, allows the molecule to recognize the Aβ.[38] In our case, the amphipathic peptide CLPFFD also has a Cys (C) residue that contains a thiol group, allowing a strong interaction with the gold surface.[39] The chemisorption of a thiol containing peptide at the gold surface could produce a stable coating that contributes to the stabilization of nanoparticles by a steric effect.

Preparation of GNR-CLPFFD. GNRs were synthesized by a seed-mediated method[22,40] (Figure 1). First, a seed solution was prepared with CTAB and $HAuCl_4$, then a cold and freshly prepared $NaBH_4$ aqueous solution was introduced to reduce

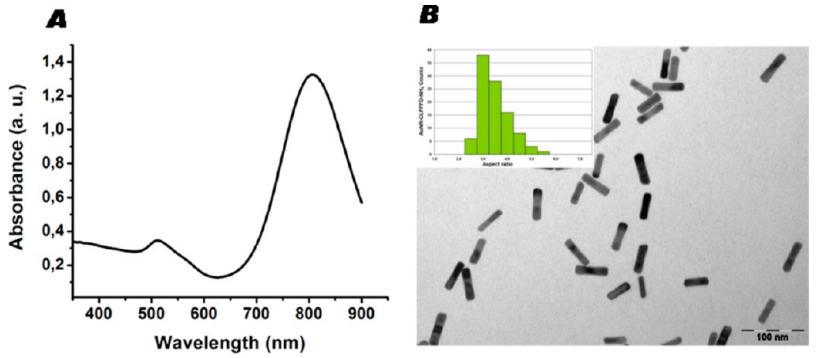

Figure 2. (A) Vis-NIR absorption spectrum of GNR-CLPFFD and (B) TEM image of GNR-CLPFFD. The inset shows the aspect ratio (length/width) in a population of 100 particles.

Au^{3+} to Au^0. The seed solution was then added to a growth solution prepared with $AgNO_3$ to control the aspect ratio, $HAuCl_4$, CTAB as template of the rod form and ascorbic acid for the reduction of Au^{3+} to Au^{1+},[41] and HCl to maintain a low pH.[42] To remove the excess of CTAB and the unreacted ions introduced during the synthesis, the GNR solution was centrifuged (first centrifugation step, Figure 1). To prepare GNR-CLPFFD, pellets (that come from 4 mL of original solution) were resuspended in 4 mL of an aqueous peptide solution in a concentration (0.25 mg/mL) that is 10 times in excess with respect to the necessary concentration to form a complete layer of peptide replacing CTAB from the nanomaterial surface. Finally the GNR-CLPFFD solution was kept at 27 °C for 72 h to complete the conjugation. For biological experiments both GNR-CLPFFD and GNR-CTAB were centrifuged for a second time (second centrifugation step, Figure 1), and pellets were resuspended in DMEM for cell viability and cell penetration experiments. To evaluate the effects of the corona protein, after the second centrifugation, samples were resuspended in plasma and incubated for 2 h at 37 °C. After that a third centrifugation step was realized and pellets were resuspended in DMEM. The treatments for biological experiments are schematized in Figure 1.

Characterization of GNR-CLPFFD. The conjugate was exhaustively characterized using Vis-NIR spectrophotometry, TEM, XPS, EELS, NAA, and amino acid analysis. Figure 2A shows the Vis-NIR spectra of the conjugate with the characteristic bands that correspond to the transverse and longitudinal plasmon resonance bands centered at 510 and 808 nm, respectively. The aspect ratio of the GNRs was found to be centered at 3.7 as was determined by TEM (Figure 2B).

In addition, EELS and XPS analyses were performed to determine the Au−S bonding in the GNR-peptide. EELS spectra in the region between 50 and 240 eV were obtained for GNRs across all samples to evaluate the presence of sulfur and ensure the functionalization of the GNRs conjugated with the peptides. In Figure 3, the sulfur EELS profile (S L2,3-edge from the 165 eV) for GNR-CLPFFD is shown. The analysis was performed after removing the background S value, as previously shown elsewhere,[43] present in both samples that was attributable to the gold surface. After this treatment, it was possible to compare the incremental value of the profile obtained in the control sample with the values obtained in the functionalized GNRs by observing how the signal is clearly superior. This increase can be attributed to the presence of sulfur atoms (S) and therefore to the presence of functionalized peptide GNRs. The red arrows show that the profile intensity

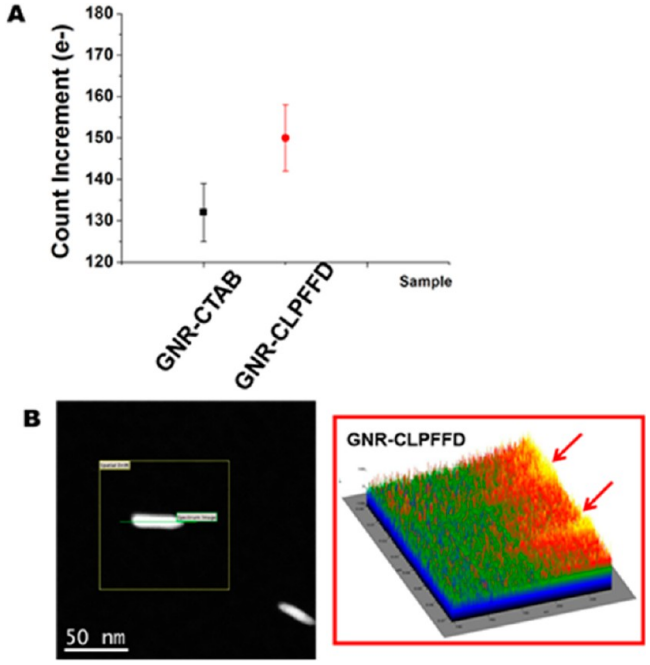

Figure 3. (A) Comparison between the control and the functionalized profiles. (B) Sulfur EELS profile the GNR-CLPFFD sample (left) and a typical HAADF STEM image (right).

increases at the ends of the GNRs, indicating that GNR-CLPFFD are most active at the ends. The observed end activity is in good agreement with the results reported by Grzelczak et al., who assume that these areas of the GNRs are not coated by silver atoms.[41] The end activity could be attributed to the crystalline composition of the face formed by Au 100 at the GNR extremes, as opposed to the middle section where Ag and AgBr are present. By using Au nanorods with the surfactant-passivating bilayer, preferential surface binding has been demonstrated for thiols that bind specifically at the tips.[44] For instance, using a thiol-modified biotin reagent, Caswell and colleagues were able to bind a molecule at the tips of the GNRs rather than homogeneously covering the entire surface.[45]

To perform XPS, the samples were lyophilized. XPS survey and high-resolution spectra were identified for GNR-CTAB and GNR-CLPFFD. The binding energies (eV) found for both are summarized in Table 1. For both types of GNRs, peaks were observed for Ag $3d_{3/2}$ and Ag $3d_{5/2}$ core levels, associated with Ag^+,[41,46] and for Au $4f_{7/2}$ and Au $4f_{5/2}$ core levels, associated with a doublet typical for Au^0. For GNR-CLPFFD, a peak was

Table 1. XPS Binding Energies (eV) of GNR-CTAB and GNR-CLPFFD

element	GNR-CTAB	GNR-CLPFFD
Au $4f_{5/2}$	83.3	84.1
Au $4f_{7/2}$	87.1	87.8
Ag $3d_{3/2}$	367.4	367.3
Ag $3d_{5/2}$	376.6	373.3
Br 3d	67.8	66.9
S $2p_{1/2}$		163.7 and 164.9
S $2p_{3/2}$		162.1 and 162.8

observed for S 2p associated with chemisorptions of sulfur grafted onto gold.[43] Table 1 summarizes the characteristic signals that correspond to GNR-CTAB and GNR-CLPFFD, and Supporting Information, Figure S2 shows the survey and high-resolution spectra for the S 2p, Ag 3d, and Au 4f spectral regions of samples taken under similar conditions. For the conjugate, expected peaks from S $2p_{1/2}$ and S $2p_{3/2}$ associated with the thiol on the gold surface, were observed (Supporting Information, Figure S3).[47−49] For the signals of GNR-CLPFFD that correspond to Au $4f_{5/2}$ and Au $4f_{7/2}$, a shift to higher energies with respect to GNR-CTAB was observed (see Supporting Information, Figure S4), which could be attributed to the chemisorption of sulfur on the gold surface.[50,51] On the other hand, the presence of Br was observed on the gold surface, which could be attributed to the presence of AgBr on the surface, as was described by Hubert et al.[51]

The number of peptides per GNR-CLPFFD was calculated by dividing the quantity of grafted peptide (obtained by performing an amino acid analysis of the GNR pellet) by the amount of GNRs in the solution, which was determined using NAA (see Experimental Section). The number of peptide molecules per GNR was 1812 ± 24. Assuming that a GNR has a cylindrical shape and a mean size of 10 × 40 nm, its corresponding area is 12,560 nm^2. The projection of a cylindrical peptide molecule (with a cylindrical base) of CLPFFD resting along its base on a gold surface in an extended conformation is 0.6 nm^2. Thus, the expected number of molecules per GNR is 21,000. It is thus possible to conclude that GNR is not completely functionalized, although the peptide concentration used was in excess with respect to GNR. As mentioned previously, the incomplete functionalization of the GNR surface could be attributed to a preferential chemisorption on the tips.[41]

Comparison between the Stability of GNR-CLPFFD and GNR-CTAB. To evaluate the stability of GNRs, we measured the Vis-NIR spectra within 72 h after obtaining the samples (after first centrifugation step and resuspension in water or peptide solution). For GNR-CTAB, a shift to lower wavelengths of the longitudinal plasmon band was observed (Figure 4). This shift could be related to an aggregation process of GNR-CTAB aligned side-by-side with a blue shift in the wavelength compared to single rods, as described for a GNR-CTAB dimer aligned side-by-side by Funston et al.[52] In contrast, the GNR-CLPFFD conjugate was stable across the same spectra with a longitudinal plasmon band centered at 808 nm, which is relevant for biological applications in photothermal therapy.

After conjugation with the peptide and subsequent centrifugation and reconstitution in water (Figure 1), the zeta potentials (Supporting Information, Figure S5) of GNR-CLPFFD and GNR-CTAB were similar (55.7 ± 2.3 mV and

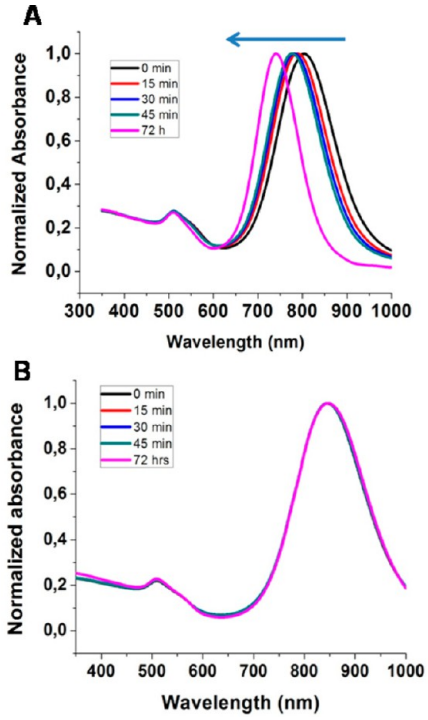

Figure 4. Vis-NIR spectra obtained after the synthesis and incubation at room temperature for 72 h to study the stability of (A) GNR-CTAB and (B) GNR-CLPFFD.

51.6 ± 2.3 mV, respectively). However, GNR-CLPFFD were more stable than GNR-CTAB. The change in stability could be attributed to a more stable capping of the GNR-peptide than that of GNR-CTAB. After removing the excess of CTAB from GNR-CTAB (first centrifugation step), the surfactant molecules could be desorbed from the surface to the solution. In contrast, in GNR-CLPFFD, peptide desorption is not favored because of chemisorption of the peptide at the gold surface, leading to stable binding (S−Au) and an increase in the steric stabilization of the colloid with respect to GNR-CTAB.

Interaction of GNR-CLPFFD with Aβ Fibrils. To characterize the interaction between the GNR-CLPFFD conjugate and Aβ fibrils, we incubated the Aβ monomer with the GNR-CLPFFD conjugate for 5 days at 37 °C to mimic physiological conditions through the formation of mature fibrils. The sample was then observed using TEM (Figure 5). In contrast with GNR-CTAB, GNR-CLPFFD shown interactions with the fibrils, which could be explained by the presence of the (Leu) L, (Phe) F, and (Phe) F hydrophobic groups in the peptides. These groups can recognize the hydrophobic nucleus, between amino acids 17−21, of Aβ. Furthermore, to determine whether the interaction of GNR-CLPFFD was selective for Aβ fibrils and not for BSA, we incubated the conjugate with BSA fibrils. No interactions with the BSA fibrils were observed in the micrographs (Supporting Information, Figure S6).

To quantitatively evaluate the attachment of each conjugate to the Aβ fibril, we centrifuged the corresponding sample at 380*g* for 20 min; under such conditions, unbound free GNR-CLPFFD remained suspended, but Aβ fibrils bound to GNRs precipitated, forming a pellet. The gold content, both in the pellets and in the supernatants, was determined by NAA. The percentage of gold bound to the fibrils was 9.2%. These results are relevant for in vivo potential applications in photothermal therapy.

dx.doi.org/10.1021/am3028537 | ACS Appl. Mater. Interfaces 2013, 5, 4076−4085

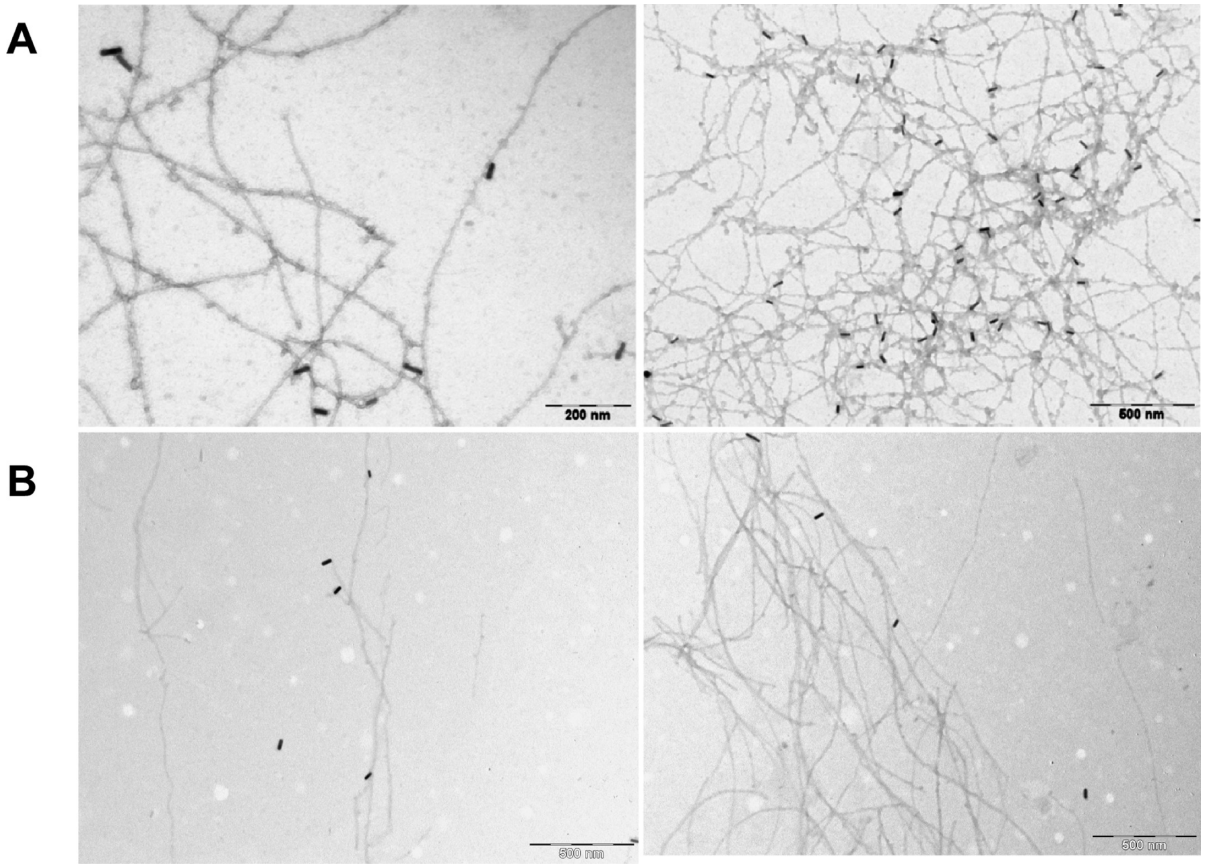

Figure 5. TEM image of Aβ fibrils and GNR-CLPFFD (A) and GNR-CTAB (B) that were incubated for 5 days. In panels A it is possible to see the attachment of the nanorods to the amyloid fibrils.

Effects of Irradiation on the Amyloidogenic Process. We prepared Aβ PIAA with high amyloidogenic capacity according to Bieschke et al.[35] The Aβ PIAA were incubated with GNR-CLPFFD, forming the complex Aβ PIAA/GNR-CLPFFD (Supporting Information, Figure S7), and a control experiment of PIAA without nanorods has been done. The samples were then irradiated with an 808 nm, 450 mW continuous laser. These complexes were irradiated for different times, and the resulting samples were incubated to evaluate whether the irradiation reduced the fibril formation process. The formation of fibrils was measured using a thioflavin-T fluorescence assay. In this assay, the amount of fibrils in suspension can be quantified by observing the intensity of the fluorescence signal, which is proportional to the amount of formed fibrils.[53] Figure 6 shows the signal from the irradiated samples, expressed as a percentage with respect to the control without irradiation and indicating a decrease in the intensity of the fluorescence signal after 2 h of irradiation (app. 40% of diminution, see fluorescence emission spectrum in Supporting Information, Figure S8) caused by the photothermal effect from the NIR irradiation. This effect was not observed in the controls (the PIAA without nanorods), as is detailed in the Supporting Information, Figure S9. In addition, we irradiated samples of PIAA that contain three different proportions of GNR-CLPFFD with respect to Aβ (0.05 nM/20 μM; 0.1 nM/20 μM; 0.2 nM/20 μM) for 2 h, and after incubation for 24 h at 37 °C, we detected a fluorescence signal in the presence of ThT, leading us to conclude that the effect is dose-dependent (see Supporting Information, Figure S10). Notably, the temperature of the bath increased by only 2 degrees after 120 min of irradiation, which is consistent with a local effect. Because the PIAA are involved in the pathogenesis, these results are very relevant in developing a new strategy to treat Alzheimer's disease based on inhibiting the formation of Aβ aggregates.

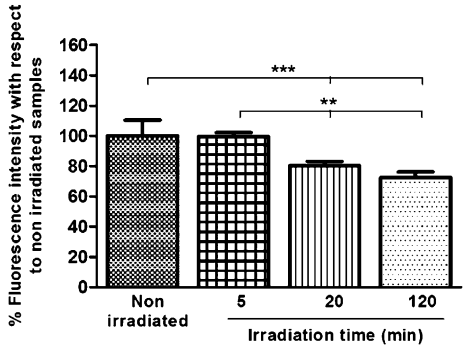

Figure 6. Normalized fluorescence intensity signal from irradiated samples of Aβ PIAA in the presence of GNR-CLPFFD, irradiated with an 808 nm, 450 mW continuous laser. Samples that were irradiated for 5, 20, and 120 min were then incubated for 24 h at 37 °C and 300 rpm, and the intensity of the fluorescence signal was measured. The results are expressed as percentages with respect to the intensity from the nonirradiated sample and represent the mean and standard deviation of $n = 4$ independent experiments (*** $p < 0.001$,** $p < 0.01$).

Cell Viability and Cell Penetration Assays. The penetration and effects on cell viability are important features that should be determined for in vivo applications. We choose

neuroblastoma SH-SY5Y cells because GNR-CLPFFD could potentially be used to treat Alzheimer's disease in the central nervous system. After confirming the stability of GNR-CLPFFD, we investigated their internalization into SH-SY5Y cells.

The effect of GNR-CLPFFD on cell viability was investigated and compared with the effect of GNR-CTAB by evaluating the viability/cytoxicity and proliferation using the MTS assay. GNR-CTAB and GNR-CLPFFD were centrifuged and resuspended in cell medium to remove excess peptide/CTAB (second centrifugation step Figure 1). In previous experiments (data not shown), we detected that, after centrifugation of GNR-CTAB and GNR-CLPFFD and reconstitution in water, the levels of free CTAB in solution were higher in GNR-CTAB than in GNR-CLPFFD (5×10^{-4} M and 5×10^{-5} M, respectively). Thus, after reconstitution in culture medium, the remaining CTAB could move into the solution. The stability of GNRs was evaluated using Vis-NIR absorption spectra observing that GNR-CTAB and GNR-CLPFFD were stable in cell media (Supporting Information, Figure S11). The GNRs were incubated with cell media at 37 °C for 24 h, and by spectrophotometry, a bathochromic shift was observed in the longitudinal plasmon peak, which could be attributed to the formation of the protein corona, as was observed for spherical GNPs capped with peptides.[43] It is well established that a protein corona forms after the interaction of nanoparticles with a biological medium with a high content of proteins. This corona has a direct influence on the toxicity and biodistribution.[54]

GNR-CLPFFD affected cell viability less compared with GNR-CTAB (Figure 7). In both samples, the remaining toxicity after reconstitution in culture cell medium could be attributed to the desorption of CTAB from the surface to the solution, as was observed by Alkilany et al.[55] However in the case of the first, the toxicity is lower possibly because of the lower concentration of CTAB.

To evaluate the effect of GNRs capped with a protein corona on cell viability, we centrifuged the GNRs (second centrifugation, Figure 1), and the pellets were resuspended in DMEM or in human plasma and were then incubated for 2 h at 37 °C. Next, the conjugates were centrifuged (third centrifugation step, Figure 1) and resuspended in DMEM to eliminate the effect of unbound proteins on the cells. Nanoparticles were stable for 24 h at 37 °C as was observed by Vis-NIR (Supporting Information, Figure S12). For GNR-CLPFFD, no significant effects on cell viability were observed; in contrast, GNR-CTAB showed a toxic effect. This result could be attributed to the desorption of CTAB molecules observed in the last sample.[55] As was mentioned previously, the CTAB content of GNR-CTAB is 1 order of magnitude greater than that of GNR-CLPFFD. In both GNRs, the protein corona is present but is not an impermeable barrier to solutes. Thus, the remaining CTAB could escape from the protein corona producing the effects on cell viability. We evaluated whether CTAB is able to diffuse and affect cell viability after centrifugation and in GNR-CLPFFD capped with the protein corona. To test this, we centrifuged the sample DMEM/DMEM (see Figure 1), and we determined the effects on cell viability in the supernatant [DMEM/DMEM (SNI)]. We observed that cell viability did not significantly change compared with respect to the control (Supporting Information, Figure S13). Additionally, to determine whether cell viability for GNR-CLPFFD was affected by the irradiation, that is,

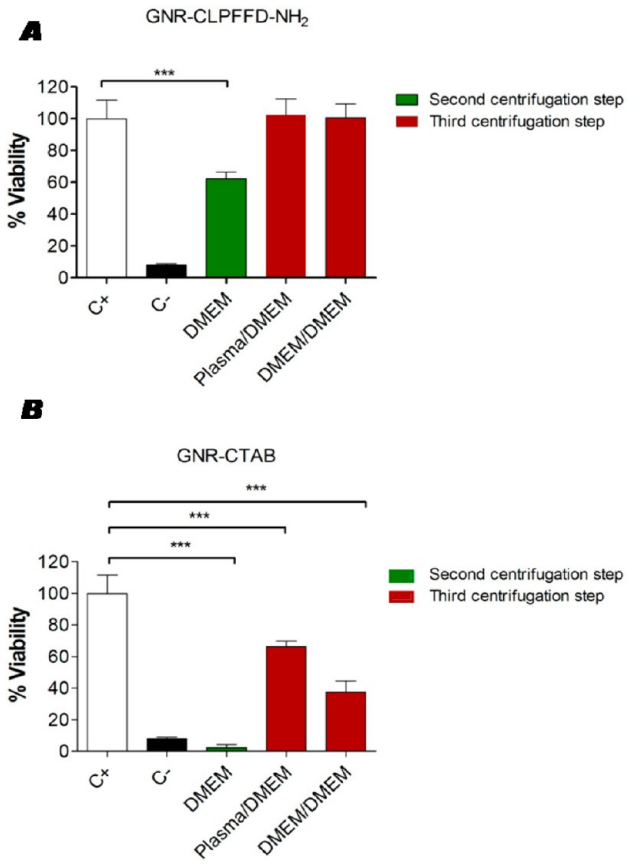

Figure 7. Cell viability assay after incubation of SH-SY5Y cells with (A) GNR-CLPFFD and (B) GNR-CTAB. The concentration of GNRs was 0.1 nM. The results are expressed as percentages compared with untreated cells and represent the mean and standard deviation of three independent experiments (*** $P < 0.001$). Cell culture media and SDS were used as negative and positive controls, respectively. DMEM refers to a sample of GNRs that was centrifuged (second centrifugation after synthesis) and resuspended in DMEM. PLASMA/DMEM refers to a sample of GNRs that was centrifuged and resuspended in human plasma before being centrifuged (third centrifugation after synthesis) and resuspended in DMEM. DMEM/DMEM corresponds to a sample of GNRs that was centrifuged and resuspended in DMEM and subsequently centrifuged and resuspended in DMEM (third centrifugation after synthesis).

CTAB would separated from the surface of the GNR-CLPFFD, a sample of GNR-CLPFFD (DMEM/DMEM, see Figure 1 and Experimental Section) was irradiated. As seen in the Supporting Information, Figure S13, the irradiation does not change the cell viability of the samples after irradiation; cell viability remained similar to that of the control. On the other hand after irradiation the supernatant of the sample DMEM/DMEM irradiated [DMEM/DMEM (SI)] did not show effects on cell viability (Supporting Information, Figure S13). This observation indicates that there is no increase in toxicity because of the release of toxic species from the GNR-CLPFFD's surface to the medium.

Cell Penetration in Neuroblastoma SH-SY5Y Cells. To visualize the internalization of the conjugate, the cells were fixed and visualized using TEM (Figure 8). GNR-CLPFFD penetrated into the cells and accumulated in vesicles. The penetration of the GNRs could be attributed to a primary interaction of the positively charged GNRs with the plasma membrane, which facilitated the electrostatic interaction with

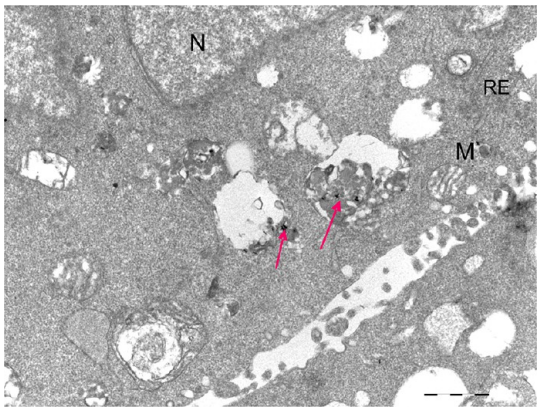

Figure 8. TEM images of SH-SY5Y cells incubated with GNR-CLPFFD 0.1 nM for 24 h at 37 °C. The red arrows indicate the presence of the nanorods inside the vesicles. M: mitochondria. N: nucleus. RE: Reticule endoplasmic.

membrane phospholipids and contributed to endocytosis.[56,57] Previous studies carried out by other authors have determined that GNRs could be endocytosed by mammalian cells and that after incorporation into the endosome could be accumulated in the cell.[58]

Effects of Irradiated PIAA with NIR in the Presence of the GNR-CLPFFD on Neurons Viability. Irradiated and nonirradiated samples of PIAA in the presence of GNR-CLPFFD were incubated with neuron cells extracted from embryo hippocampal rats (E18). This system and MTS assay are helpful to show the toxic effect of Aβ and its inhibition.[59,60] Nonirradiated samples of PIAA-GNR-CLPFFD exhibited a diminution of cell viability (app. 40%) with respect to the control (Figure 9) while the same irradiated samples did not show effects on cell viability with respect to the controls.

We designed a biologically functional GNR-peptide plasmonic conjugate and demonstrated improved nanoparticle stability and reduced effects on cell viability, although penetration of the nanomaterials into cells was observed. The

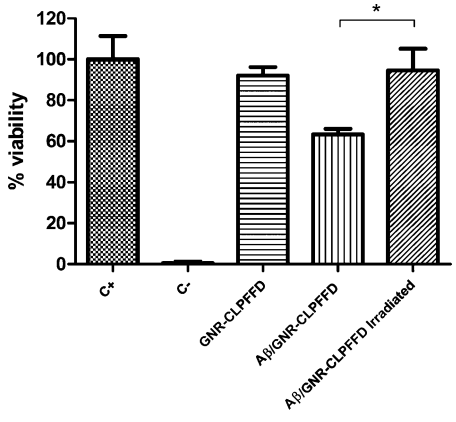

Figure 9. Cell viability assay after incubation of embryo hippocampal neurons incubated with PIAA irradiated and nonirradiated in the presence of GNR-CLPFFD. PIAA were irradiated for 2 h and then incubated with the cells for 24 h at 37 °C. The final concentration of Aβ is 10 μM and GNR-CLPFFD is 0.04 nM. The results are expressed as percentages compared with untreated cells and represent the mean and standard deviation of three independent experiments (* $p < 0.05$). Cell culture media (Neurobasal) and SDS were used as negative and positive controls, respectively. The GNR-CLPFFD control is 0.04 nM.

increased stability could be attributed to the chemisorption of the peptide. The resultant capping of the GNR-CLPFFD conjugate is more stable than that of GNR-CTAB. Furthermore, the NIR irradiation of the PIAA mixed with the Aβ PIAA/GNR-CLPFFD contributed to the reduction in the formation of Aβ amyloid fibrils and to reduce its cytotoxicity. The resultant conjugates retained their unique optical properties under culture cell conditions. Therefore, we expect that GNR-CLPFFD could have applications in therapeutics for Alzheimer's disease.

■ ASSOCIATED CONTENT

Ⓢ Supporting Information

Peptides HPLC, X-ray photoelectron spectroscopy, Z-potential values, stability of conjugates in plasma, and DMEM and TEM micrographs of albumin fibrils. Normalized fluorescence intensity signal from irradiated samples of different proportions of Aβ PIAA with respect to GNR-CLPFFD. Cell viability assay after incubation of SH-SY5Y cells with GNR-CLPFFD irradiated. This material is available free of charge via the Internet at http://pubs.acs.org.

■ AUTHOR INFORMATION

Corresponding Author

*E-mail: mkogan@ciq.uchile.cl.

Notes

The authors declare no competing financial interest.

■ ACKNOWLEDGMENTS

We thank to Dr. Carmen Lopez and Dr. Nancy Olea for discussion of TEM images. We thank to Dr. Alejandra Alvarez and David Chamorro for their help in the toxicity assays with hippocampus neurons. This work was partially supported by AECID, Fondecyt 1090143, Fondecyt 1130425, Anillo ACT-95, MECESUP-0811: CICYT (CTQ2012-30930), the Generalitat de Catalunya (2009SGR 1024), the Institute for Research in Biomedicine, and the Barcelona Science Park. C.A. is grateful to MECESUP, CONICYT, and Vicerrectoría USACH for fellowships. A.R. is thankful for a Postdoctoral Fellowship of CONICYT (Fondecyt 3130654). We thank to Estela Martin for assessment with laser manipulation.

■ REFERENCES

(1) Marcon, L.; Stievenard, D.; Melnyk, O. *Bioconjugate Chem.* **2008**, *19*, 802−805.
(2) Katz, E.; Willner, I. *Angew. Chem., Int. Ed.* **2004**, *43*, 6042−6108.
(3) Kogan, M. J.; Olmedo, I.; Hosta, L.; Guerrero, A. R.; Cruz, L. J.; Albericio, F. *Nanomedicine* **2007**, *2*, 287−306.
(4) Kim, J.; Park, S.; Lee, J. E.; Jin, S. M.; Lee, J. H.; Lee, I. S.; Yang, I.; Kim, J. S.; Kim, S. K.; Cho, M. H.; Hyeon, T. *Angew. Chem., Int. Ed.* **2006**, *45*, 7754−7758.
(5) Panyam, J.; Zhou, W. Z.; Prabha, S.; Sahoo, S. K.; Labhasetwar, V. *FASEB J.* **2002**, *16*, 1217−1226.
(6) Kogan, M. J.; Bastus, N. G.; Amigo, R.; Grillo-Bosch, D.; Araya, E.; Turiel, A.; Labarta, A.; Giralt, E.; Puntes, V. F. *Nano Lett.* **2006**, *6*, 110−115.
(7) El-Sayed, I. H.; Huang, X. H.; El-Sayed, M. A. *Nano Lett.* **2005**, *5*, 829−834.
(8) Yguerabide, J.; Yguerabide, E. E. *J. Cell Biochem.* **2001**, *84*, 71−81.
(9) Karhanek, M.; Kemp, J. T.; Pourmand, N.; Davis, R. W.; Webb, C. D. *Nano Lett.* **2005**, *5*, 403−407.
(10) Taton, T. A.; Lu, G.; Mirkin, C. A. *J. Am. Chem. Soc.* **2001**, *123*, 5164−5165.

(11) Kohler, N.; Sun, C.; Wang, J.; Zhang, M. Q. *Langmuir* **2005**, *21*, 8858−8864.
(12) Yang, P. H.; Sun, X. S.; Chiu, J. F.; Sun, H. Z.; He, Q. Y. *Bioconjugate Chem.* **2005**, *16*, 494−496.
(13) Hirsch, L. R.; Stafford, R. J.; Bankson, J. A.; Sershen, S. R.; Rivera, B.; Price, R. E.; Hazle, J. D.; Halas, N. J.; West, J. L. *Proc. Natl. Acad. Sci. U.S.A.* **2003**, *100*, 13549−13554.
(14) Kogan, M. J.; Araya, E.; Olmedo, I.; Bastus, N. G.; Guerrero, S.; Puntes, V. F.; Giralt, E. *Nanoscale Res. Lett.* **2008**, *3*, 435−443.
(15) Huo, Q.; Triulzi, R. C.; Dai, Q.; Zou, J. H.; Leblanc, R. M.; Gu, Q.; Orbulescu, J. *Colloids Surf., B* **2008**, *63*, 200−208.
(16) Barnes, D. E.; Yaffe, K. *Lancet Neurol.* **2011**, *10*, 819−823.
(17) Mullerhill, B.; Beyreuther, K. *Annu. Rev. Biochem.* **1989**, *58*, 287−307.
(18) Crouch, P. J.; Harding, S. M. E.; White, A. R.; Camakaris, J.; Bush, A. I.; Masters, C. L. *Int. J. Biochem. Cell B* **2008**, *40*, 181−198.
(19) Estrada, L. D.; Soto, C. *Curr. Top. Med. Chem.* **2007**, *7*, 115−126.
(20) El-Sayed, M. A.; Huang, X. H.; Neretina, S. *Adv. Mater.* **2009**, *21*, 4880.
(21) Weissleder, R. *Nat. Biotechnol.* **2001**, *19*, 316−317.
(22) Nikoobakht, B.; El-Sayed, M. A. *Chem. Mater.* **2003**, *15*, 1957−1962.
(23) Broderick, G.; Michael Craig, W. *J. Dairy Sci.* **1989**, *72*, 2540−2548.
(24) Cortesi, R.; Esposito, E.; Menegatti, E.; Gambari, R.; Nastruzzi, C. *Int. J. Pharm.* **1996**, *139*, 69−78.
(25) van Ruissen, F.; Le, M.; Carroll, J. M.; van der Valk, P. G. M.; Schalkwijk, J. *J. Invest. Dermatol.* **1998**, *110*, 358−363.
(26) Huff, T. B.; Hansen, M. N.; Zhao, Y.; Cheng, J. X.; Wei, A. *Langmuir* **2007**, *23*, 1596−1599.
(27) Niidome, Y.; Honda, K.; Higashimoto, K.; Kawazumi, H.; Yamada, S.; Nakashima, N.; Sasaki, Y.; Ishida, Y.; Kikuchi, J. *Chem. Commun.* **2007**, 3777−3779.
(28) Takahashi, H.; Niidome, T.; Kawano, T.; Yamada, S.; Niidome, Y. *J. Nanopart. Res.* **2008**, *10*, 221−228.
(29) Connor, E. E.; Mwamuka, J.; Gole, A.; Murphy, C. J.; Wyatt, M. D. *Small* **2005**, *1*, 325−327.
(30) Lee, S. E.; Sasaki, D. Y.; Perroud, T. D.; Yoo, D.; Patel, K. D.; Lee, L. P. *J. Am. Chem. Soc.* **2009**, *131*, 14066−14074.
(31) Didychuk, C. L.; Ephrat, P.; Belton, M.; Carson, J. J. L. *Proc. SPIE* **2008**, *6856*, 68560M1−68560M8.
(32) Orendorff, C. J.; Alam, T. M.; Sasaki, D. Y.; Bunker, B. C.; Voigt, J. A. *ACS Nano* **2009**, *3*, 971−983.
(33) MacQueen, A. *The 2007 NNIN REU Research Accomplishments* **2007**, 32−33.
(34) Link, S.; El-Sayed, M. A. *J. Chem. Phys.* **2001**, *114*, 2362−2368.
(35) Bieschke, J.; Siegel, S. J.; Fu, Y. W.; Kelly, J. W. *Biochemistry* **2008**, *47*, 50−59.
(36) Goy-Lopez, S.; Juarez, J.; Alatorre-Meda, M.; Casals, E.; Puntes, V. F.; Taboada, P.; Mosquera, V. *Langmuir* **2012**, *28*, 9113−9126.
(37) Zhuohua, Z.; Henrike, H.; Viet Minh, D.; Dorothee, A.; Christine, S.-P.; Matthias, S.; Bernd, S.; Marc van de, W.; Hans, C.; Paul, S.; Bart, De, S.; Xi, H.; Bruce, A. Y. *Nature* **1998**, *395*, 698−702.
(38) Soto, C.; Sigurdsson, E. M.; Morelli, L.; Kumar, R. A.; Castano, E. M.; Frangione, B. *Nat. Med.* **1998**, *4*, 822−826.
(39) Tielens, F.; Santos, E. *J. Phys. Chem. C* **2010**, *114*, 9444−9452.
(40) Jana, N. R.; Gearheart, L.; Murphy, C. J. *Chem. Mater.* **2001**, *13*, 2313−2322.
(41) Grzelczak, M.; Perez-Juste, J.; Mulvaney, P.; Liz-Marzan, L. M. *Chem. Soc. Rev.* **2008**, *37*, 1783−1791.
(42) Tiwari, N.; Kalele, S.; Kulkarni, S. K. *Plasmonics* **2007**, *2*, 231−236.
(43) Olmedo, I.; Araya, E.; Sanz, F.; Medina, E.; Arbiol, J.; Toledo, P.; Alvarez-Lueje, A.; Giralt, E.; Kogan, M. J. *Bioconjugate Chem.* **2008**, *19*, 1154−1163.
(44) Sethi, M.; Pacardo, D. B.; Knecht, M. R. *Langmuir* **2010**, *26*, 15121−15134.
(45) Caswell, K. K.; Wilson, J. N.; Bunz, U. H. F.; Murphy, C. J. *J. Am. Chem. Soc.* **2003**, *125*, 13914−13915.
(46) Gunawan, C.; Teoh, W. Y.; Marquis, C. P.; Lifia, J.; Amal, R. *Small* **2009**, *5*, 341−344.
(47) Vericat, C.; Benitez, G. A.; Grumelli, D. E.; Vela, M. E.; Salvarezza, R. C. *J. Phys.: Condens. Matter* **2008**, *20*, 184004.
(48) Lau, K. H. A.; Huang, C.; Yakovlev, N.; Chen, Z. K.; O'Shea, S. J. *Langmuir* **2006**, *22*, 2968−2971.
(49) Jiang, P.; Xie, S. S.; Yao, J. N.; Pang, S.; Gao, H. J. *J. Phys. D: Appl. Phys.* **2001**, *34*, 2255−2259.
(50) Brust, M.; Walker, M.; Bethell, D.; Schiffrin, D. J.; Whyman, R. *J. Chem. Soc., Chem. Commun.* **1994**, 801−802.
(51) Hubert, F.; Testard, F.; Spalla, O. *Langmuir* **2008**, *24*, 9219−9222.
(52) Funston, A. M.; Novo, C.; Davis, T. J.; Mulvaney, P. *Nano Lett.* **2009**, *9*, 1651−1658.
(53) Levine, H. *Protein Sci.* **1993**, *2*, 404−410.
(54) Dobrovolskaia, M. A.; Patri, A. K.; Zheng, J. W.; Clogston, J. D.; Ayub, N.; Aggarwal, P.; Neun, B. W.; Hall, J. B.; McNeil, S. E. *Nanomed. Nanotechnol.* **2009**, *5*, 106−117.
(55) Alkilany, A. M.; Nagaria, P. K.; Wyatt, M. D.; Murphy, C. J. *Langmuir* **2010**, *26*, 9328−9333.
(56) Wang, L. M.; Liu, Y.; Li, W.; Jiang, X. M.; Ji, Y. L.; Wu, X. C.; Xu, L. G.; Qiu, Y.; Zhao, K.; Wei, T. T.; Li, Y. F.; Zhao, Y. L.; Chen, C. Y. *Nano Lett.* **2011**, *11*, 772−780.
(57) Pujals, S.; Fernandez-Carneado, J.; Lopez-Iglesias, C.; Kogan, M. J.; Giralt, E. *Biochim. Biophys. Acta, Biomembr.* **2006**, *1758*, 264−279.
(58) Chanda, N.; Shukla, R.; Katti, K. V.; Kannan, R. *Nano Lett.* **2009**, *9*, 1798−1805.
(59) Yaar, M.; Zhai, S.; Panova, I.; Fine, R. E.; Eisenhauer, P. B.; Blusztajn, J. K.; Lopez-Coviella, I.; Gilchrest, B. A. *Neuropathol. Appl. Neurobiol.* **2007**, *33*, 533−543.
(60) Xue, D.; Zhao, M.; Wang, Y.-j.; Wang, L.; Yang, Y.; Wang, S.-w.; Zhang, R.; Zhao, Y.; Liu, R.-t. *Neurobiol. Dis.* **2012**, *46*, 701−709.